Electronic Supplementary Material (ESI) for Energy & Environmental Science.

Supporting Information

Nitrogen-Doped Cobalt Phosphate@Nanocarbon Hybrids for Efficient Electrocatalytic Oxygen Reduction

*Tianhua Zhou, Yonghua Du, Shengming Yin, Xuezeng Tian, Hongbin Yang, Xin Wang, Bin Liu, Haimei Zheng, Shizhang Qiao*and Rong Xu**

Material

All solvents and chemicals were obtained from commercial supplies and used directly as received unless otherwise stated. KOH, graphite, $Co_3(PO_4)_2 \cdot xH_2O$, L-proline, cobalt(II) nitrate hexahydrate, Nafion® 117 solution (~5% in a mixture of lower aliphatic alcohols and water) were purchased from Sigma-Aldrich. Potassium permanganate was obtained from Sinopharm Chemical Reagent Co., Ltd. Commercial Pt/C catalyst (20 wt% Pt on Vulcan carbon black) was obtained from Johnson Matthey. SH_3LCo was synthesized according to the reported procedure.[1]

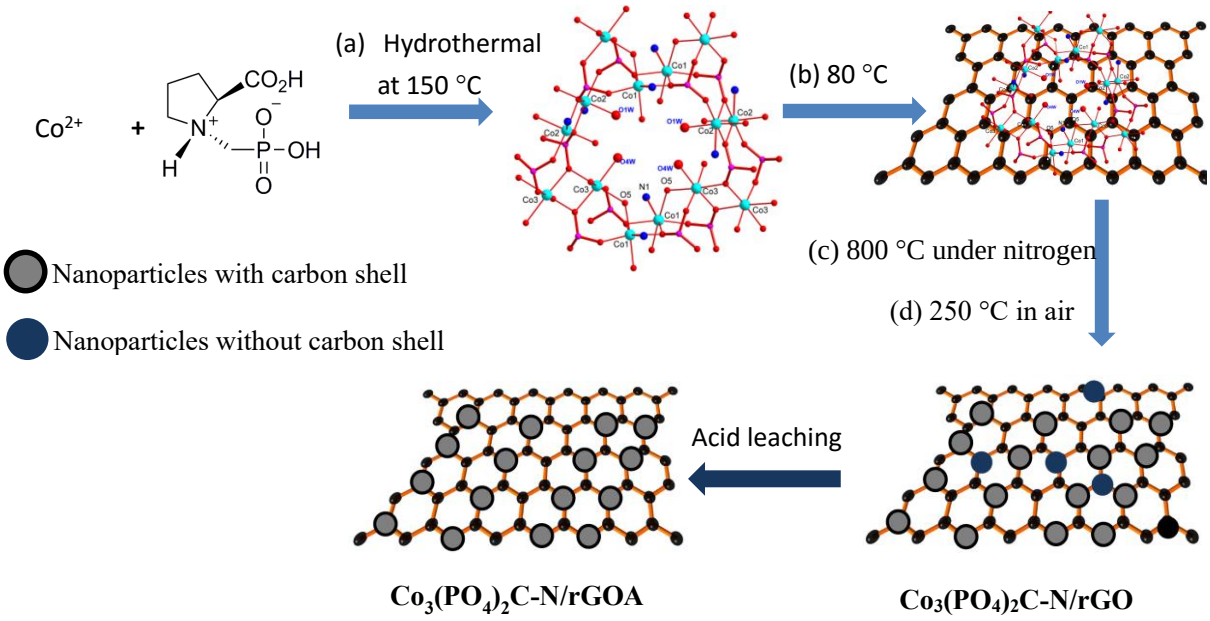

Scheme 1. Synthesis procedure of $Co_3(PO_4)_2$C-N/rGOA.

Method

Synthesis $Co_3(PO_4)_2$C-N/rGOA hybrid materials

Graphene oxide (GO) was first prepared according to the reported procedure.[2] Then 0.02 g of GO was dispersed in 40 mL of deionized water to 5 mg/mL of GO solution. Next 0.05 g of SH_3LCo was added to the aqueous solution of GO and the mixture was sonicated for 30 min. Afterward, the mixture was heated to 80 °C with stirring to remove the solvent and the obtained powder was further dried in an oven at 60 °C. Then the powder mixture of SH_3LCo and GO was pyrolyzed at 800 °C for 3 h under N_2 atmosphere, followed by calcination in air at 250 °C for 1.5 h to afford the final $Co_3(PO_4)_2$C-N/rGO hybrid catalyst. To remove any surface contamination including carbon-free cobalt phosphate, the sample was further stirred at room temperature in 50 mL of 2.0 M HCl solution for 12 h and then was washed with deionized water until neutral pH was obtained. Finally, the black powder denoted

$Co_3(PO_4)_2$C-N/rGOA was obtained after freeze drying. For comparison, the $Co_3(PO_4)_2$C-NA catalyst was prepared by direct pyrolysis of metal-organic phosphonate SH_3LCo in the absence of GO to give $Co_3(PO_4)_2$C-N which was then washed using HCl solution. $Co_3(PO_4)_2$C/rGOA was prepared with the same procedure as that of $Co_3(PO_4)_2$C-N/rGOA except with $Co_3(O_2CCH_2CH_2PO_3)_2 \cdot 6H_2O$ crystal obtained from 3-phosphonopropionic acid (PPAH3)[1, 3] as the precursor. $Co_3(PO_4)_2$/rGOA was fabricated by using commercial $Co_3(PO_4)_2$ substitution for SH_3LCo whereas Co_4NC was obtained by direct pyrolysis of cobalt(II) phthalocyanine.

Characterization

Powder X-ray diffraction (XRD) patterns were obtained on a Bruker AXS D2 Advanced X-ray diffractometer with monochromatized Cu Ka radiation (λ = 1.54056 Å, 40 kV and 20 mA). The data were collected with 2θ in a range of 5°-65° and a step size of 0.02°/0.5 s. All measurements were performed at room temperature and atmospheric pressure. The surface component of cobalt was analyzed by X-ray photoelectron spectroscopy (XPS) performed on a Thermo Scientific ESCALAB 250 and the binding energies were calibrated using the C 1s peak at 285.0 eV. Transmission electron microscopy (TEM) was performed on JEOL JEM-3010 and JEM-2100. The contents of the Co were detected with an inductively coupled plasma-optical emission spectroscopy (ICP-OES, Perkin Elemer Optima 8300, MA, US) after dissolving the samples with a mixture of HCl and HNO_3 (3/1 v/v). Co K-edge X-ray absorption near-edge structure (XANES) and extended X-ray absorption fine structure (EXAFS) spectra were recorded at the 1W2B beamline of the Beijing synchrotron radiation facility (BSRF). Raman spectra were collected using a Micro-Raman spectrometer system (in Via, Renishaw, UK) coupled with a microscope (Alpha 300, WITec, Germany) in a backscattering geometry using 514 nm (Renishaw, UK). FTIR spectra were obtained with a Perkin Elmer FTIR Spectrum GX using KBr technique in the range of 4000–400 cm^{-1}. The surface area (BET) of all samples were measured by N_2 adsorption and desorption at 77 K using a Quantachrome Autosorb-6 sorption system. The samples were degassed offline at 150 °C for 24 h under vacuum before the analysis.

Electrochemical measurements

The electrochemical measurements were carried out at room temperature on an Autolab PGSTAT302N potentiostat/galvanostat using a standard three-electrode system. The catalyst coated on glassy carbon rotating disk electrode (diameter 5 mm) was used as a working electrode. A platinum plate and Ag/AgCl electrode with 3.5 M KCl solution were employed as the counter and reference electrodes, respectively. All the potentials used in this work were reported with respect to the reversible hydrogen electrode (RHE). Glassy carbon electrodes were polished

before each experiment with 0.05 μm polishing alumina (Ultrafine Alumina Slurry, Pine Research Instrumentation, USA), and ultrasonically cleaned thoroughly with deionized water, ethanol, acetone, and deionized water.

To prepare the working electrode, 5 mg of catalysts and 15 μL of 5 wt% Nafion solutions were dispersed in 1 mL of 3:1 v/v water/isopropanol mixed solvent under sonication to form a homogeneous ink. Subsequently, 10 μL of the catalyst ink was dropped onto the surface of the glass carbon rotating disk electrode and dried at room temperature under air to produce a uniform film with a catalyst loading of 0.25 mg cm^{-2}. The loading of commercial Pt/C was 0.1 mg cm^{-2} (20 μg_{Pt} cm^{-2}). Cyclic voltammetry (CV) was performed in argon and O_2-saturated 0.1 M and 1.0 M KOH electrolyte with a scan rate of 20 mV s^{-1}. Before each experiment, the working electrode was continuously cycled at least 40 times between 0 and 1.0 V at a scan rate of 100 mV s^{-1} until a stable CV was recorded. Rotating disk electrode (RDE) experiments were conducted in O_2-saturated electrolyte at a scan rate of 5 mV/s and different rotation speeds (400-2025 rpm) controlled by Pine Modulated Speed Rotator (MSR). The electrolyte was saturated with O_2 before each experiment and a gentle flow of O_2 was maintained during the measurement. The electron transfer number (n) during oxygen reduction reaction was calculated at various electrode potential according to the Koutecky-Levich equation,

$$\frac{1}{J} = \frac{1}{J_L} + \frac{1}{J_K} = \frac{1}{B\omega^{1/2}} + \frac{1}{J_K} \quad (1)$$

$$B = 0.62nFC_0(D_0)^{2/3}\nu^{-1/6} \quad (2)$$

$$J_K = nFKC_0 \quad (3)$$

$$J_L = 0.62nFC_0(D_0)^{2/3}\nu^{-1/6}\omega^{1/2} \quad (4)$$

where J represents the measured current density, J_K and J_L are the kinetic- and diffusion-limiting current densities, ω is the angular velocity ($\omega = 2\pi N$, N is the linear rotation speed), n is the overall transferred electron number in oxygen reduction reaction, F is the Faraday constant (F = 96485 C mol^{-1}), C_0 is the bulk concentration of O_2 (1.2×10^{-6} mol cm^{-3}) in 0.1 M KOH electrolyte while C_0 is 7.8×10^{-7} mol cm^{-3} in 1.0 M KOH (7.8×10^{-7} mol cm^{-3}) , D_0 is the O_2 diffusion coefficient in 0.1 M KOH electrolyte (1.9×10^{-5} cm^2 s^{-1}) while D_0 is 1.8×10^{-5} cm^2 s^{-1} in 1.0 M KOH, ν is the kinematic viscosity of the electrolyte (0.01 cm^2 s^{-1}), and k is the electron transfer rate constant. According to equation (4), the theoretical limiting current density can be calculated to be 5.7 mA cm^{-2} whereas in 1.0 M KOH the value is 3.57 mA cm^{-2}. For the Tafel plots, the kinetic current was determined from the mass-transport correction of RDE by

$$J_K = \frac{J \times J_L}{(J_L - J)}$$

To detect H_2O_2 yield, rotating ring-disk electrode (RRDE) measurements were conducted with the disk electrode at a scan rate of 5 mV s^{-1}. The ring potential was set to 1.5 V in 0.1 M KOH, 1.3 V in 1.0 M KOH to oxidize H_2O_2 transferred from glass carbon disk electrode. The H_2O_2 yield and electron transfer number (n) were calculated by following equations:

$$HO_2^- = 200 \times \frac{I_r/N}{I_d + I_r/N}$$

$$n = 4 \times \frac{I_d}{I_d + I_r/N}$$

Where I_d and I_r are disk current and ring current, respectively, and N is the ring collection efficiency. N was determined to be 0.33 from the reduction of $K_3Fe[CN]_6$.

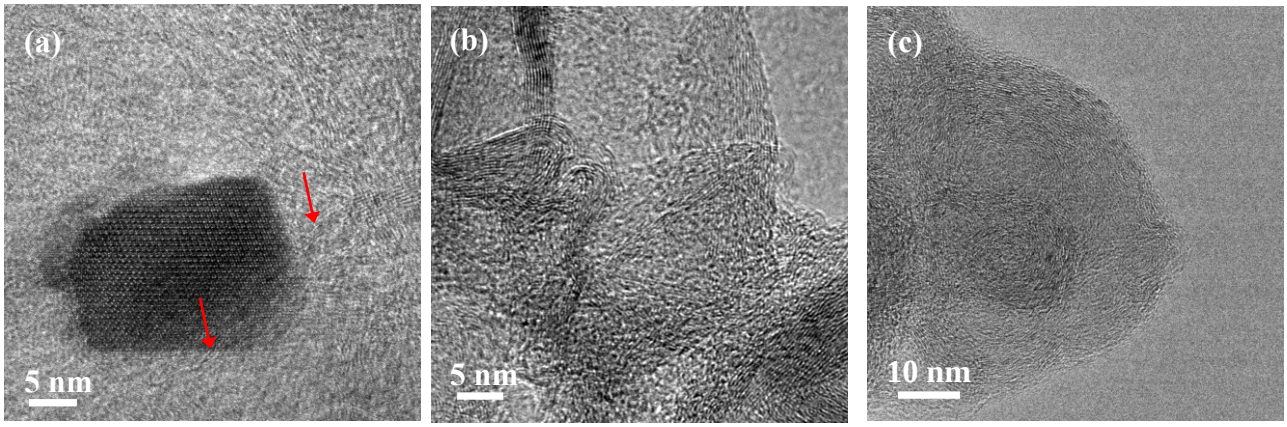

Figure S1. Micrographs of $Co_3(PO_4)_2$C-N/rGOA. (a) HRTEM image. (b) HRTEM images of graphitic carbon and (c) hollow carbon shells. The red arrows point the graphitic carbon shell decorating nanoparticles.

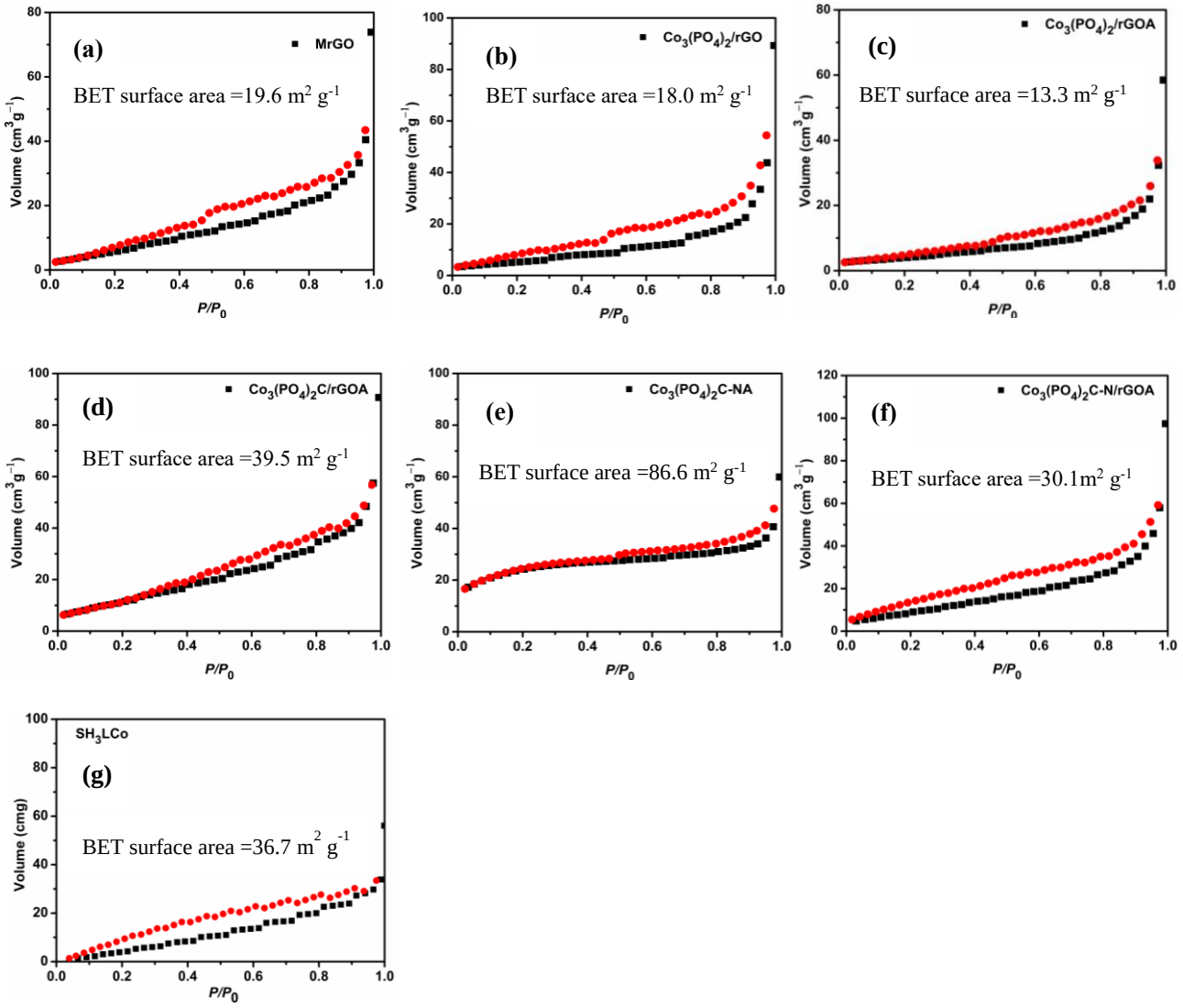

Figure S2. Nitrogen adsorption-desorption isotherm of (a) Mildly oxidized rGO (MrGO), (b) $Co_3(PO_4)_2$/rGO, (c) $Co_3(PO_4)_2$/rGOA, (d) $Co_3(PO_4)_2$C/rGOA, (e) $Co_3(PO_4)_2$C-NA, (f) $Co_3(PO_4)_2$C-N/rGO, and (g) the precursor SH_3LCo.

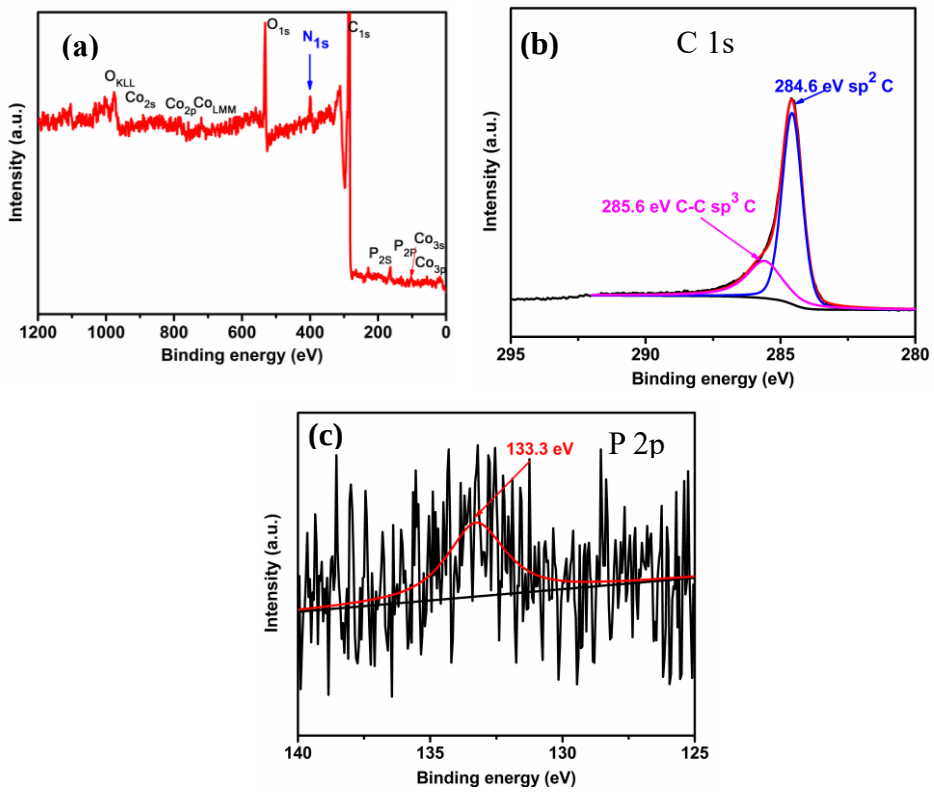

Figure S3. (a) XPS survey spectrum of $Co_3(PO_4)_2$C-N/rGOA and high-resolution XPS spectra of (b) C 1s, and (c) P 2p.

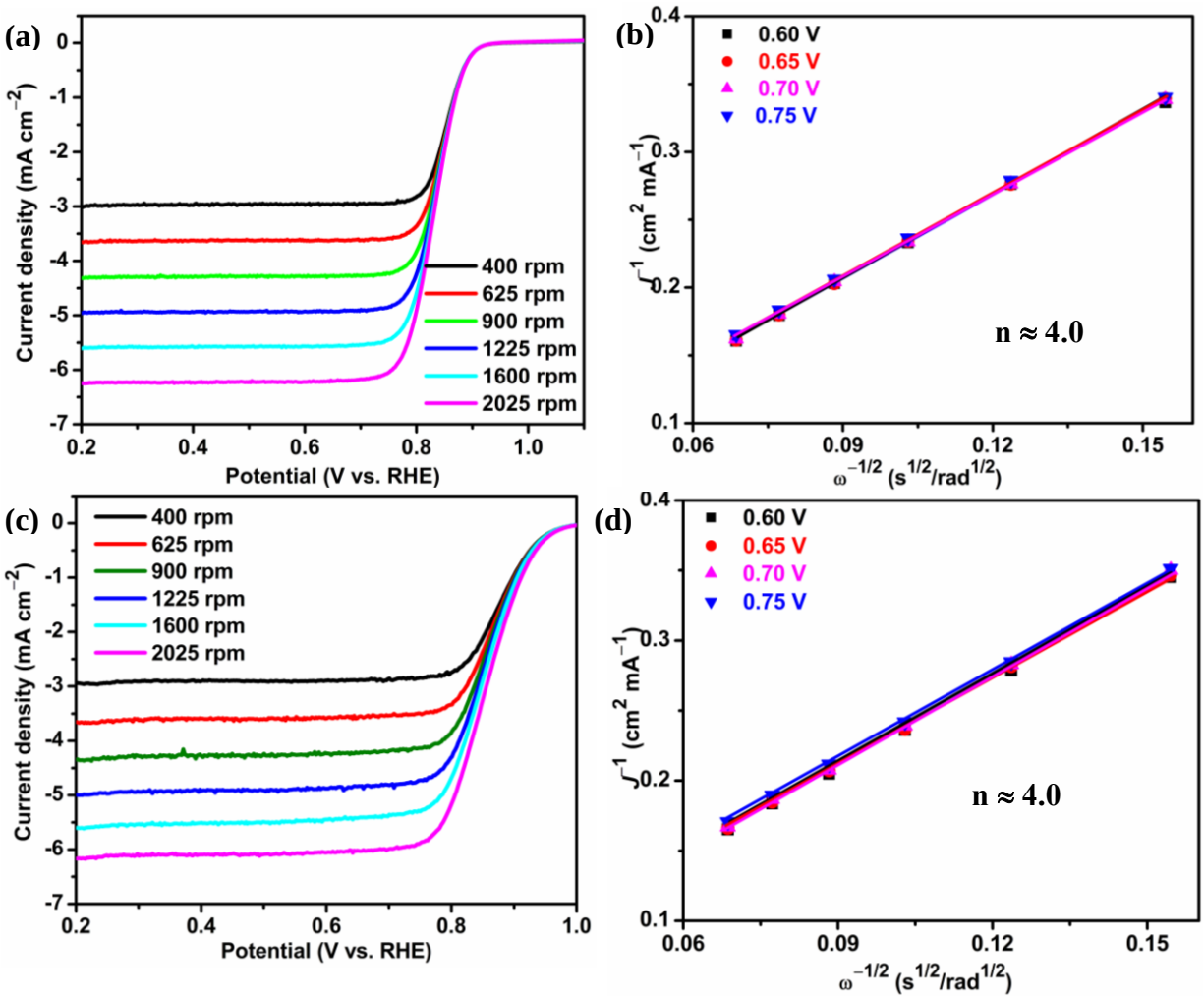

Figure S4. RDE for $Co_3(PO_4)_2$C-N/rGOA (a) and Pt/C (c), and the corresponding Koutecky-Levich plots derived from RDE measurement for $Co_3(PO_4)_2$C-N/rGOA (b) and Pt/C (d). All data were collected in O_2-saturaed 0.1 M KOH solution at a scan rate of 5 mV s^{-1}. The loading of catalysts was 20 μg_{pt} cm^{-2} for Pt/C.

Table S1. Kinetic current density based on Koutecky-Levich plots derived from RDE measurement (Figure S4) at different potential.

Compounds	Kinetic current density (mA cm^{-2})			
	0.75 V	0.70 V	0.65 V	0.60V
$Co_3(PO_4)_2$C-N/rGOA	38.46	45.41	51.02	46.21
Pt/C	37.17	47.59	46.57	47.62

Table S2. Summary of the electrochemical properties of the catalysts investigated in O_2-saturated 0.1 M KOH solution with a loading of 0.25 mg cm^{-2} and a potential window of 0.2 V versus RHE (all data are obtained via LSV at a rotation rate of 1600 rpm).

Electrocatalyst	Onset potential (V vs. RHE)	Limiting current density (mA cm^{-2})	Half-wave potential (V vs. RHE)	Electron transfer number at 0.6 V vs. RHE
PNrGO	0.797	3.58	0.594	3.2 at 0.4V
$Co_3(PO_4)_2$C-N/rGOA	0.962	5.58	0.837	4.01
Pt/C	1.008	5.60	0.851	4.08

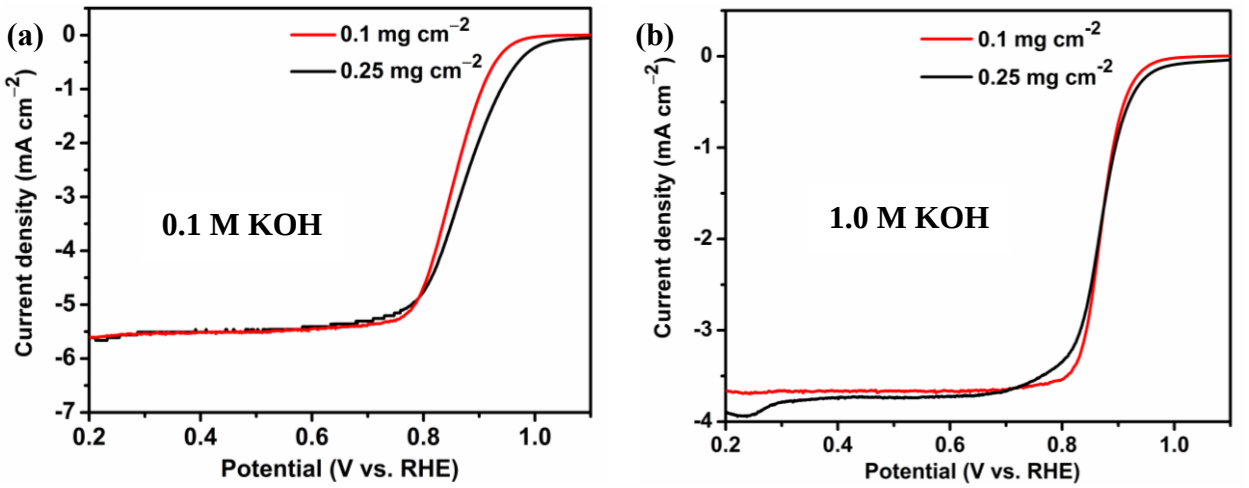

Figure S5. LSV curves of the commercial Pt/C catalyst at different loadings in 0.1 M KOH (a) and 1.0 M KOH (b) solutions.

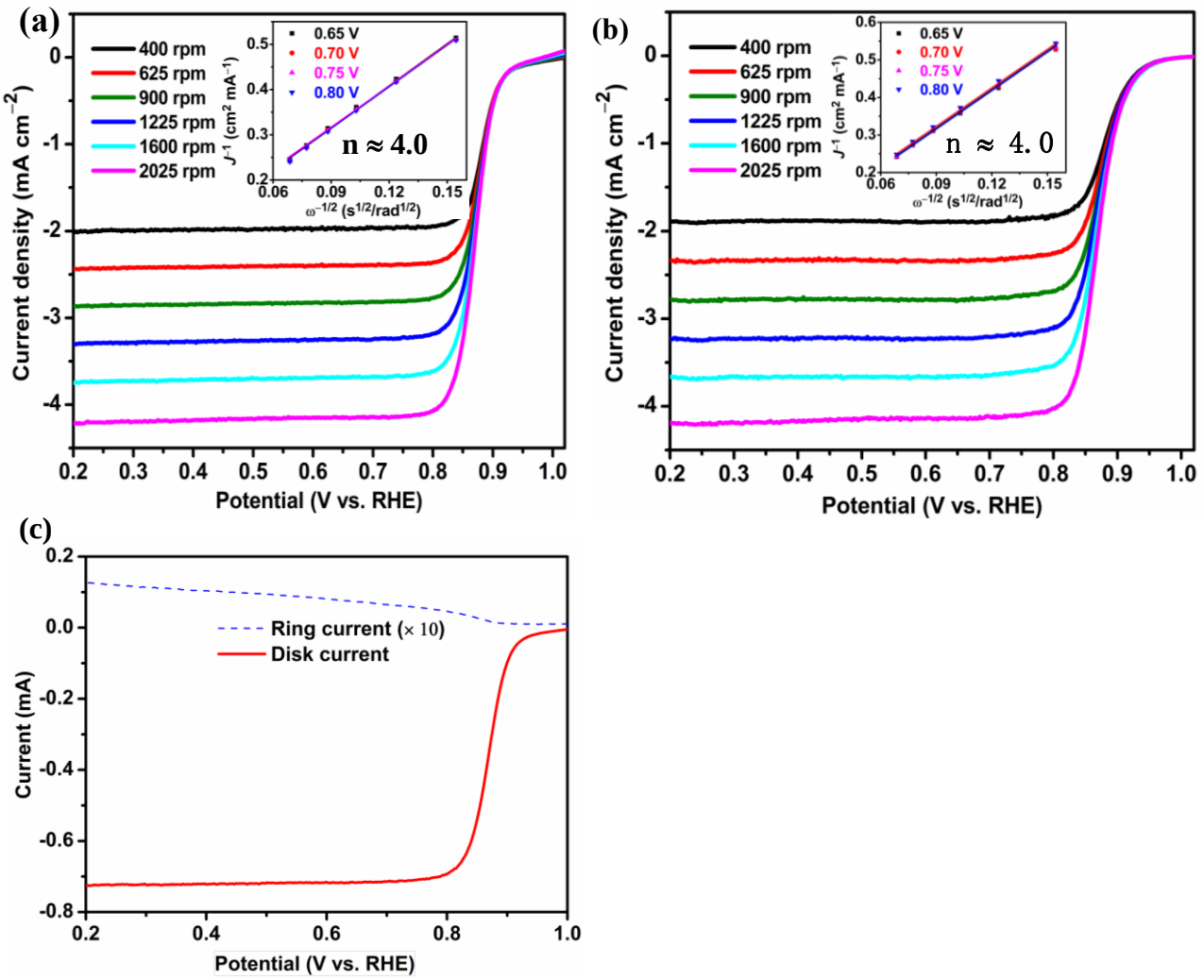

Figure S6. RDE for $Co_3(PO_4)_2$C-N/rGOA (a) and Pt/C (b), and the corresponding Koutecky-Levich plots derived from RDE measurement for $Co_3(PO_4)_2$C-N/rGOA (inset Figure S6a) and Pt/C (inset Figure S6b). RRDE curves of $Co_3(PO_4)_2$C-N/rGOA in O_2-saturated 1.0 M KOH solution at 1600 rpm (c). The ring potential was constant at 1.3 V versus RHE. All data were collected in O_2-saturaed 1.0 M KOH solution at a scan rate of 5 mV s^{-1}. The loading of catalysts was 20 μg_{pt} cm^{-2} for Pt/C.

Table S3. Summary of the electrochemical properties of the catalysts investigated in O_2-saturated 1.0 M KOH solution with a loading of 0.25 mg cm^{-2} and a potential window of 0.2 V versus RHE (all data are obtained via LSV at a rotation rate of 1600 rpm).

Electrocatalyst	Onset potential (V vs. RHE)	Limiting current density (mA cm^{-2})	Half-wave potential (V vs. RHE)	Electron transfer number at 0.7 V vs. RHE
$Co_3(PO_4)_2$/rGO				
$Co_3(PO_4)_2$/rGOA	0.86	1.69	0.73	-[a]
$Co_3(PO_4)_2$C/rGOA	0.89	2.75	0.77	2.46
$Co_3(PO_4)_2$C-NA	0.94	3.34	0.83	4.07
$Co_3(PO_4)_2$C-N/rGOA	0.97	3.75	0.87	4.08
Pt/C	1.00	3.67	0.87	4.11

Note: [a] The data do not follow first-order kinetics and cannot adapt the classical Koutecky-Levich model to analyze the result.

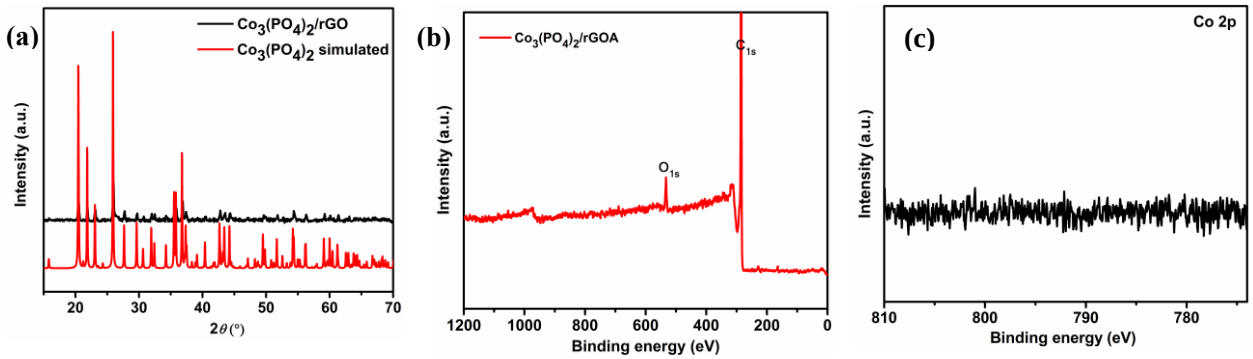

Figure S7. (a) XRD of $Co_3(PO_4)_2$/rGO before acid etching, and (b) XPS survey spectrum of $Co_3(PO_4)_2$/rGOA after acid etching of $Co_3(PO_4)_2$/rGO and high-resolution XPS spectra of (c) Co 2p.

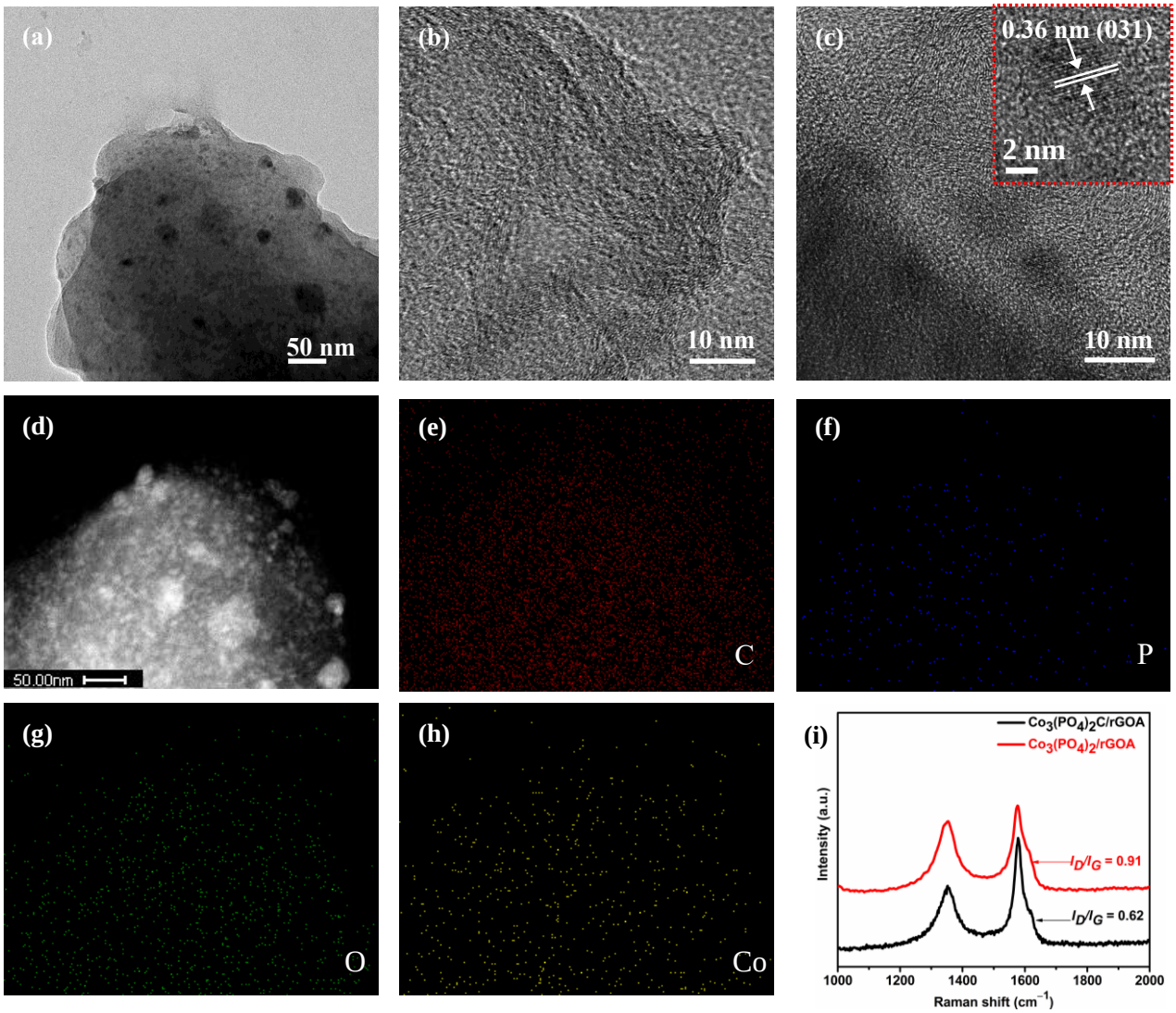

Figure S8. (a)TEM, (b-c) HRTEM, and (d) STEM and the corresponding elemental mapping images (e-h) of $Co_3(PO_4)_2C$/rGOA showing the element distributions of C, P, O, and Co. (i) Raman spectra of $Co_3(PO_4)_2C$/rGOA and $Co_3(PO_4)_2$/rGOA (λ_{ex} at 514 nm). Note: $Co_3(PO_4)_2C$/rGOA shows a small I_D/I_G ratio (0.62) in comparison with that of $Co_3(PO_4)_2$/rGOA without graphitic carbon in situ formed (0.91), indicating that more ordered carbon formed in former due to the introduction of graphitic carbon during thermal treatment, confirmed by TEM (Figure S8b-c).

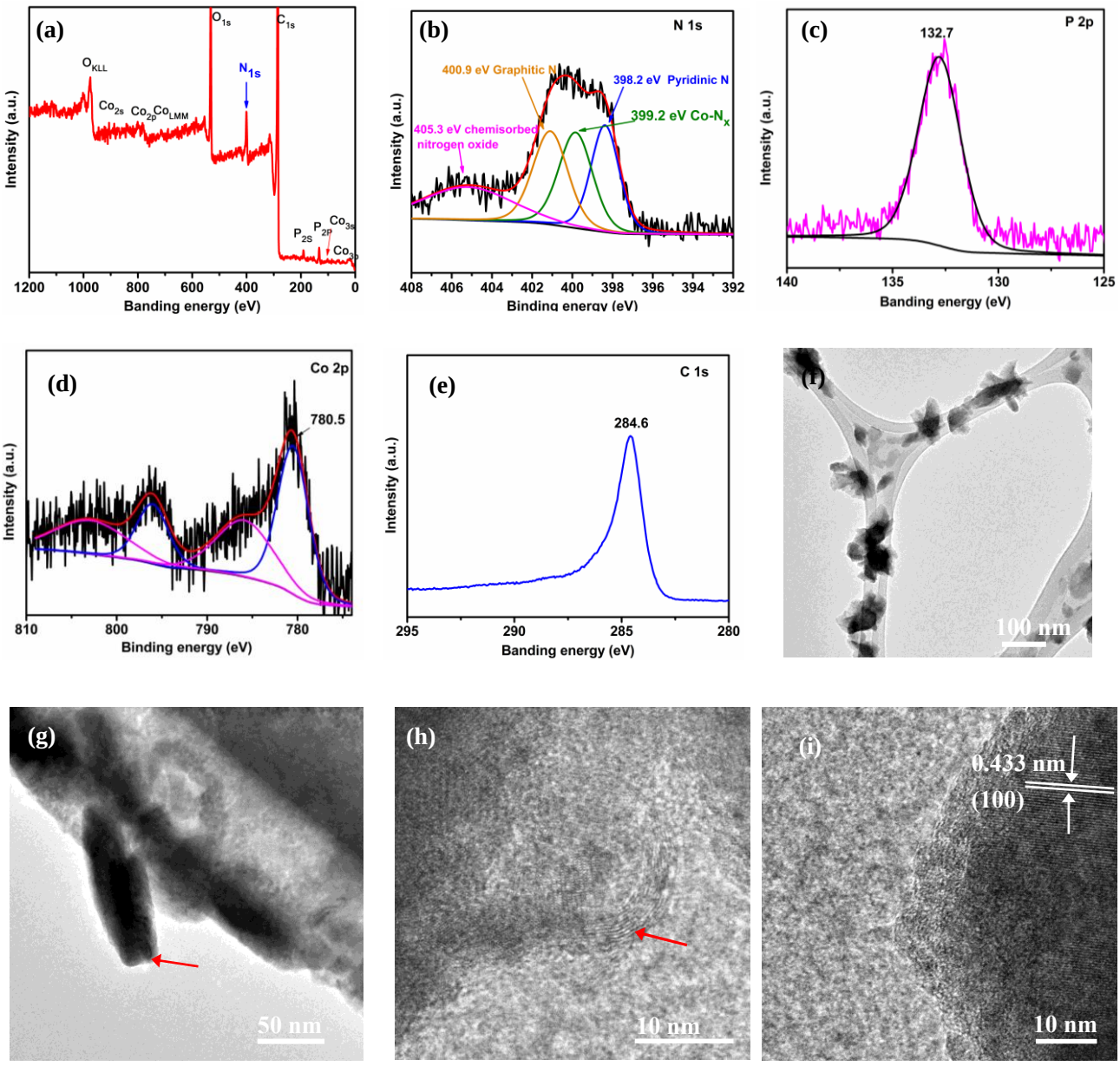

Figure S9. (a) XPS survey spectrum of $Co_3(PO_4)_2$C-NA and high-resolution XPS spectra of (b) N 1s, (c) P 2p, (d) Co 2p, and (e) C 1s, (f-i) TEM and HRTEM of $Co_3(PO_4)_2$C-NA. Red arrows designate rod-like nanoparticle (Figure S9g) and graphitic carbon (Figure S9h), respectively.

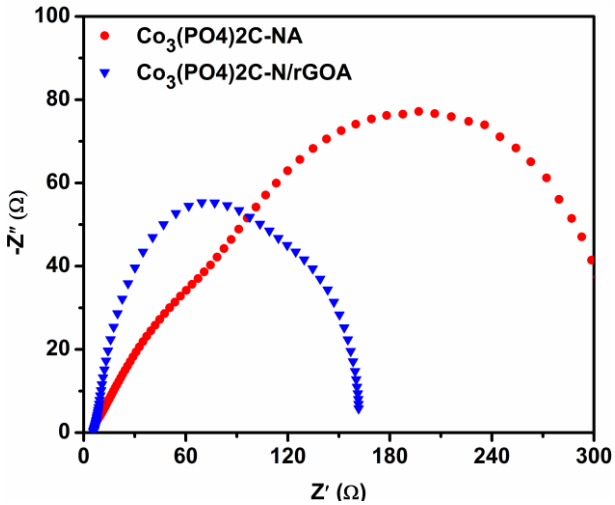

Figure S10. Nyquist plots of $Co_3(PO_4)_2C$-NA and $Co_3(PO_4)_2C$-N/rGOA at 0.85 V with a rotation rate of 1600 rpm.

Table S4. Comparison of ORR performance of the highly active transition-metal catalysts reported recently with $Co_3(PO_4)_2C$/rGO.

Sample	Electrolyte	Onset potential (V)	Half-wave potential (V)	Limiting current density (mA cm^{-2})	Electron transfer number (*n*)	Reference
$Co_3(PO_4)_2C$-N-HA/rGO	0.1 M KOH	0.962	0.837	5.58	4.01	This work
$Co_3(PO_4)_2C$-N-HA/rGO	1.0 M KOH	0.968	0.872	3.75	4.08	This work
$MnCo_2O_4$/N-rmGO	1.0 M KOH	0.95	N.A	~3.75	3.9	[4]
CoO/NCNT	1.0 M KOH	0.93	N.A	~3.75	3.9	[5]
Co_3O_4/N-doped-graphene	0.1 M KOH	0.88	0.83	~5.0	4.0	[2]
Fe−N/C-800	0.1 M KOH	0.923	0.809	6.06	4.15	[6]
Co@Co_3O_4@C-CM	0.1 M KOH	0.93	0.81	N.A.	3.8-3.9	[7]
N-doped covalent organic polymers	0.1 M KOH	N.A.	0.78	N.A.	3.9	[8]
CoP-CMP800 [a]	0.1 M KOH	-0.12	-0.18	4.62	3.85	[9]
Fe-P-C	0.1 M KOH	0.95	N.A.	5.01	3.61	[10]
N-Fe-CNT/CNP(0.2mgcm^{-2}) at 20 mVs-1, 900rpm	0.1 M NaOH	>1.05	0.87±0.01	<3.5	4.0	[11]
P-doped graphite	0.1 M KOH	0.1	N.A.	4.3[b]	3.0	[12]
FePc-Py-CNTs at 10 mVs^{-1}	0.1 M KOH	<1.0	0.915	N.A	4.0	[13]

Note: [a] V vs. AgCl/Ag, Electron transfer number was obtained at -0.35 V; [b] the current density was obtained at a rotation rate of 1100 rpm.

Table S5. Structure fit parameters from Co-edge EXAFS spectra analysis of $Co_3(PO_4)_2$C-N/rGOA.

Sample	Pair	N	R(Å)	σ^2(Å^2)
$Co_3(PO_4)_2$C-N/rGOA	Co-O	5±0.3	1.99±0.01	0.004±0.0007
	Co-N	0.9±0.2	2.23±0.01	0.002±0.0005

N: coordination number. R: bond distance. σ^2: Debye-Waller factor.

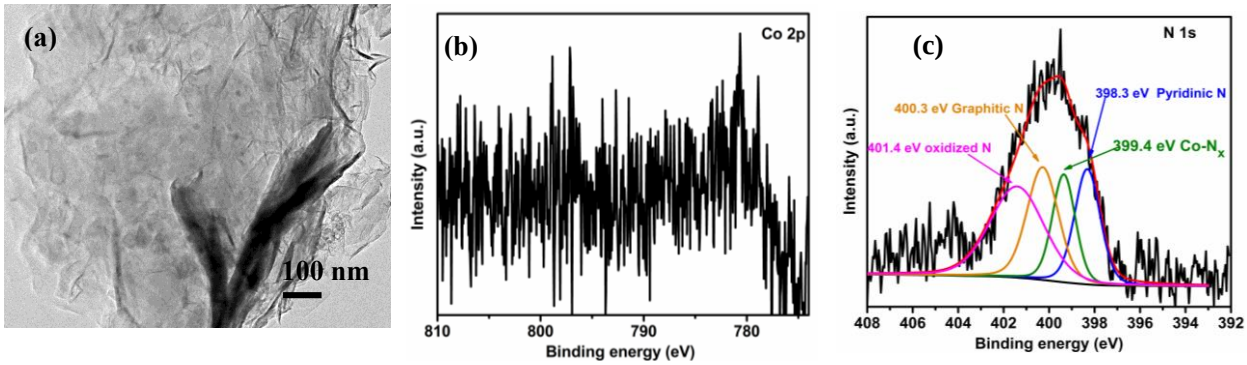

Figure S11. (a) TEM, and (b) high-resolution XPS spectra of Co 2p and (c) N 1s for second acid-etched $Co_3(PO_4)_2$C-N/rGOA .

References:

1. T. Zhou, D. Wang, S. Chun-Kiat Goh, J. Hong, J. Han, J. Mao and R. Xu, *Energy Environ. Sci.*, 2015, **8**, 526-534.
2. Y. Liang, Y. Li, H. Wang, J. Zhou, J. Wang, T. Regier and H. Dai, *Nat. Mater.*, 2011, **10**, 780-786.
3. A. Distler and S. C. Sevov, *Chem. Commun.* 1998, 959-960.
4. Y. Liang, H. Wang, J. Zhou, Y. Li, J. Wang, T. Regier and H. Dai, *J. Am. Chem. Soc.*, 2012, **134**, 3517-3523.
5. Y. Liang, H. Wang, P. Diao, W. Chang, G. Hong, Y. Li, M. Gong, L. Xie, J. Zhou, J. Wang, T. Z. Regier, F. Wei and H. Dai, *J. Am. Chem. Soc.*, 2012, **134**, 15849-15857.
6. L. Lin, Q. Zhu and A.-W. Xu, *J. Am. Chem. Soc.*, 2014, **136**, 11027-11033.
7. W. Xia, R. Zou, L. An, D. Xia and S. Guo, *Energy Environ. Sci.*, 2015, **8**, 568-576.
8. Z. Xiang, D. Cao, L. Huang, J. Shui, M. Wang and L. Dai, *Adv. Mater.* 2014, **26**, 3315-3320.
9. Z.-S. Wu, L. Chen, J. Liu, K. Parvez, H. Liang, J. Shu, H. Sachdev, R. Graf, X. Feng and K. Müllen, *Adv. Mater.* 2014, **26**, 1450-1455.
10. K. P. Singh, E. J. Bae and J.-S. Yu, *J. Am. Chem. Soc.*, 2015, **137**, 3165-3168.
11. H. T. Chung, J. H. Won and P. Zelenay, *Nat Commun*, 2013, **4**, 1922-1928.
12. Z.-W. Liu, F. Peng, H.-J. Wang, H. Yu, W.-X. Zheng and J. Yang, *Angew. Chem. Int. Ed*, 2011, **50**, 3257-3261.
13. R. Cao, R. Thapa, H. Kim, X. Xu, M. Gyu Kim, Q. Li, N. Park, M. Liu and J. Cho, *Nat Commun*, 2013, **4**, 2076-2082.